SHORT-TERM BEHAVIORS AND DESIGN EQUATIONS OF MORTARLESS REINFORCED CONCRETE MASONRY WALLS

Sittichai Seangatith*

Received: Oct 8, 2004; Revised: Apr 26, 2005; Accepted: May 26, 2005

Abstract

This paper presents the results of a study of the short-term behavior of mortarless reinforced concrete masonry wall subjected to two types of loading: concentrated axial load and transverse load. The specimens were made of standard hollow concrete masonry units, reinforcing steel bars, and grout. The variables studied were steel reinforcement ratio, height or span of the specimen, and grouting pattern. A total of 40 specimens were tested, including 24 specimens under concentrated axial load and 16 specimens under transverse load. The experimentally obtained results were correlated to the ACI 530-99 design equations for a reinforced mortar jointed wall and statistical analyses were performed. Finally, the design equations were adjusted based on the obtained results.

Keyword: Mortarless masonry, masonry wall, concrete masonry unit, concentrated load, transverse load

Introduction

Mortarless masonry or dry-stacked masonry differs from traditional masonry in that no mortar is used in the construction. Historical evidence at fort Porta Nigra, Tier, Germany, shows that this concept originated about 1,800 years ago (Marzahn, 1999). This Roman fortified gateway was constructed using sandstone blocks without any mortar. Recently, this concept has been used in many countries such as Germany and USA due to the developments in masonry unit production leading to well leveled units with small tolerances of size and shape. Typically, the units used in mortarless masonry are the same as those used in masonry with a thin mortar layer. Sometimes, they are in the form of interlocked masonry units to ensure the interlocking between them. The units can be both solid and hollow masonry units. Solid block units are popular in Europe, while hollow concrete block units, which are stacked and grouted with or without reinforcement afterward, are popular in USA (Marzahn, 2000). Construction with mortarless masonry is an attractive alternative to conventional masonry with mortar joints due to the construction efficiency and economy. It eliminates the use of mortar in head joint and bed joint, reducing the material and labor costs as well as cutting the mortar curing time. It also requires less skilled labor and the masonry units can be laid easier and quicker, offering labor cost and time savings. However, in the construction of mortarless masonry structural components such as wall, pilaster, and column, the first course has to be stacked carefully in grout or mortar because the absence of the mortar layer may affect the plumb and level of these structural components.

School of Civil Engineering, Institute of Engineering, Suranaree University of Technology, Nakhon Ratchasima 30000 Thailand

* *Corresponding author*

Suranaree J. Sci. Technol. 12(3):178-192

Marzahn (1997, 2000) performed experimental investigation on the structural behavior of dry-stacked masonry and mortar-jointed masonry walls subjected to uniform compression perpendicular to the bed plane. The experimental setup consisted of masonry specimens with five units high and two units wide, according to German standard DIN 18554, and five units high and one unit wide. The specimens were made of solid calcium silicate units and autoclaved aerated concrete units. The surfaces of the units were machined to create different bedding conditions. A thin mortar layer was used to build the mortar-jointed masonry specimens. In comparison with the mortar-jointed masonry wall, initial deformation of the dry-stacked masonry wall had a larger volume of the plastic parts, indicating that the masonry units have to settle down in order to balance uneven surfaces before they can carry loads. This initial deformation was observed up to about 30% of the compressive strength of the wall. The compressive strength of the dry-stacked masonry wall was up to 85 - 95% of that of the mortar jointed masonry wall. This lower strength is mainly due to the quality of the unit such as differences in height and uneven bed surface between each unit. The dry-stacked masonry wall failed differently from the mortar jointed masonry wall. It failed in a similar way to concrete and the collapse occurred by formation of a shearing line in a diagonal direction, while the mortar jointed masonry failed in the form of wall splitting in the plane of the wall. It was also concluded that the bedding conditions have little effect in decreasing the compressive strength of the dry-stacked masonry walls.

In developing countries, the demand for low-cost buildings, such as houses, farm buildings, warehouses, and small industrial buildings, is high. These buildings should be high-quality permanent structures so that maintenance is minimal and they should be produced in a short time to catch up with increasing need. Recently, the use of the load-bearing concrete masonry wall is increasingly popular due to its low-cost and ease of building into any shape. In addition, due to the advantages of the mortarless masonry as previously mentioned, the concept of mortarless reinforced concrete masonry wall built by using typical concrete masonry units has been proposed and studied. This paper presents the results of a study on the short-term behavior of the masonry wall subjected to concentrated axial load and transverse load. Grout and steel reinforcement were used in this study, since there is no interlocking between the concrete masonry units. Twenty-four wall specimens were tested under concentrated axial load and sixteen wall specimens were tested under transverse load. The experimental results were correlated to the ACI 530-99 design equations for a reinforced mortar jointed wall and the correlations were statistically analyzed. Finally, the design equations were adjusted and proposed.

Mechanical Properties of the Component and Masonry

All masonry walls were constructed using standard hollow load-bearing concrete masonry units laid in running bond, grouted with coarse grout, and reinforced with steel reinforcing bars. The concrete unit had actual dimensions of 390 mm long by 190 mm high and 140 mm thick with dimension tolerances of less than $\pm$3 mm as specified in ASTM C90. The grout had a mix proportion as specified in ASTM C476 (Type I Portland cement: fine aggregate: coarse aggregate of 1: 2.25: 2 by volume) and slump in the range of 250 and 280 mm. Samples of the masonry units and grout were taken and tested at regular intervals throughout this testing program. Two types of mortarless prism, partially grouted and fully grouted, were also built and tested to determine the compressive strength and modulus of elasticity of the mortarless masonry. Table 1 presents the summary of the geometric and mechanical properties of the concrete masonry unit, grout, and prism. Steel reinforcing bars were the same as those used in reinforced concrete work specified in ASTM A615. Table 2 shows the yielding stresses, allowable compressive stresses, and allowable tensile stresses of the reinforcing bars, respectively.

In order to compare the behavior and the compressive strength of the mortarless and mortar-jointed masonry prisms, two types of

mortar-jointed prisms, partially grouted and fully grouted, were also built using type N mortar (1: 3 cement: sand by volume) with 120 percent flow and tested as specified in ASTM C270. Type N mortar was used to provide a lower bound to the results. The test results are shown in Table 1. In comparison, the partially grouted and fully grouted mortarless prisms had a compressive strength of 85% and 92% of those of the partially grouted and fully grouted mortar-jointed prisms, respectively. The mortarless prisms had a larger initial deformation in the first load level, up to 35% of the compressive strength, compared to about 15% of that of the mortar-jointed prisms as shown in Figure 1. These results are similar to those reported by Marzahn (Marzahn, 1999). By preloading the prism specimens to 30% of their compressive strength, it was observed that the initial deformations were reduced significantly upon reloading. The failure mode of these two types of prisms, however, was similar in the form of wall splitting in their own plane as shown in Figure 2.

Since there is no building code for the design of mortarless reinforced concrete masonry walls, the masonry wall specimens used in this study were preliminarily designed and detailed in accordance with ACI 530-99. Tables 3 and 4 show the details of the specimens for the concentrated axial load test and the transverse

Table 1. Geometric and mechanical properties of concrete unit, grout, and prism

	Dimensions (l)(h)(t) (mm)	Test method	No. of specimens	Compressive strength		Modulus of elasticity (GPa)
				Mean (MPa)	COV (%)	
Concrete unit	(390)(190)(140)	ASTM C140	24	9.62	8.1	-
Grout	190 mm cube	ASTM C1019	24	16.51	10.6	-
Partially grouted mortarless prism	(390)(570)(140)	ASTM E447	9	8.58	11.9	4.88
Fully grouted mortarless prism	(390)(570)(140)	ASTM E447	9	12.98	11.4	5.42
Partially grouted prism	(390)(590)(140)	ASTM E447	9	9.80	11.7	-
Fully grouted prism	(390)(590)(140)	ASTM E447	9	14.03	11.7	-

Note: (1) the compressive strengths were calculayed using net cross-sectional area of 27,900 mm^2 for concrete unite, 41,250 mm^2 forpartially grouted prisms, and 54,600 mm^2 for fully grouted prisms.

(2) Partialy grouted prism is the prism havingg one hollow cell grouted and the fully grouted prism is the prism having both of the rtwo cells grouted.

Table 2. Yielding stress and allowable strees of reinforcing bares

Type	Test method	Yielding (MPa)	Allowable compressive stress (MPa)	Allowable tensile stress (MPa)
RB9	ASTM E8	328.3	131	140
DB12	ASTM E8	356.4	142	140
DB16	ASTM E8	445.9	165	165

load test, respectively. They were three-unit wide by four-, thirteen-, and fifteen-course high, which were considered large enough to be representative of the walls. In each type of the tests, the specimens were constructed in four groups having the cross-sections as shown in Figure 3. All specimens were built in the laboratory by an experienced mason using normal construction procedures and were air-cured for at least 28 days before testing. Two specimens were tested for each specimen number. The specimen identification number has the following meanings: the first letter and number indicate type of testing (C for concentrated axial load test, F for transverse load test) and specimen group, the second number indicates specimen height or span, and the last letter indicates grouting pattern (P for partial grouting, F for fully grouting). For example, C1-076-P is the specimen for concentrated axial load test, group 1, 0.760 m high, and partially grouted. It should be noted that, for the concentrated axial load test, the reinforcement ratio, ρ, is the ratio of the total reinforcing bar area in one masonry unit to the net cross-sectional area of the masonry with one unit wide. For the transverse load test, the reinforcement ratio is half of the value for the concentrated axial load test because the compressive reinforcing bars are close to the neutral axis of the specimens, hence, only the tensile reinforcing bars were considered to effectively resist the applied load. The slenderness ratio is the height of the specimen, h, divided by the minimum radius of gyration, r, of its cross-section.

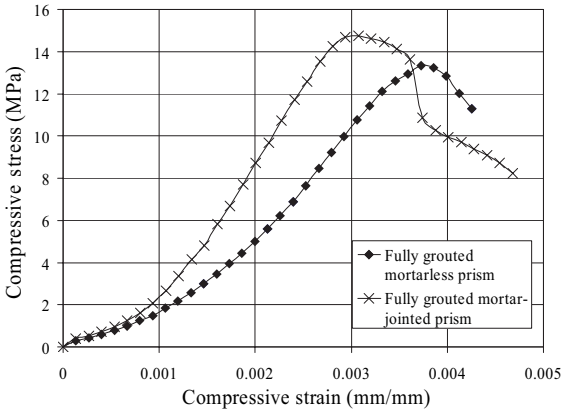

Figure 1. Compressive stress-strain curves of masonry prisms

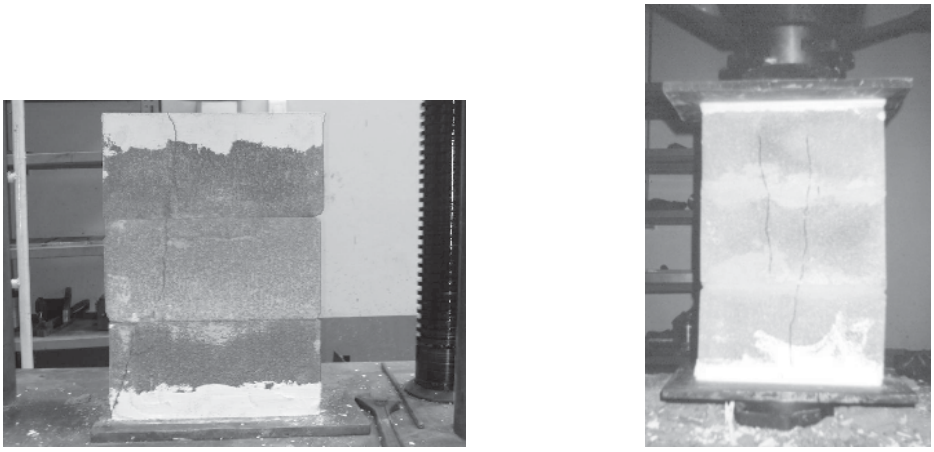

a) M ortarless prism b) Mortar-jointed prism

Figure 2. Typical cracks in masonry prisms

Test Set-up

Figures 4 and 5 show the test set-up for the concentrated axial load test and for the transverse load test, respectively. The loading frame was used to apply the loads to the specimens. For the concentrated load test, the axial load was applied through a steel bearing plate 200 mm wide, 150 mm long, and 25 mm thick. This gives a bearing load-area ratio (the ratio of the area of the bearing plate to the total cross-sectional area of the specimens) of 12.8%. The bearing plate was set lengthwise on a plaster bed on the top of the specimens at one of the grouted cells near the centerline of the specimen and connected to the hydraulic ram by a hinged support as shown in Figure 4(b). The bottom end was set directly on a thin layer of plaster on the reaction floor. The axial deformation at the loading point and the lateral deflection at the mid-height were monitored by two dial gages at each location. For the transverse load test, the specimens were supported by two rigid steel beams, having the same length as the specimen width, at both ends. Due to support configuration, the spans of the specimens were equal to the overall length subtracted by 0.010 m. The specimens were subjected to the four-point loading at one-third point of the span using the load-transferring system as shown in Figure 5(b). The lateral deflection at the mid-span was

Table 3. Details of test specimen for concentrated axial load test

Specimen number	Reinforcing bars for 1 grouted cell	Reinforcement ratio, ρ (%)	Height, h (m)	Slendernes ratio, h/r	Grouting pattern	No. of specimen
C1-076-P	2-DB12	0.55	0.76	17.3	Partial	2
C1-247-P	2-DB12	0.55	2.47	56.4	Partial	2
C1-285-P	2-DB12	0.55	2.85	65	*Partial*	*2*
C2-076-P	2-RB9	0.47	0.76	18.8	Full	2
C2-247-P	2-RB9	0.47	2.47	61.1	Full	2
C2-285-P	2-RB9	0.47	2.85	70.5	Full	2
C3-076-P	2-DB16	0.97	0.76	17.3	Partial	2
C3-247-P	2-DB16	0.97	2.47	56.4	Partial	2
C3-285-P	2-DB16	0.97	2.85	65	Partial	2
C4-076-P	2-DB12	0.83	0.76	18.8	Full	2
C4-247-P	2-DB12	0.83	2.47	61.1	Full	2
C4-285-P	2-DB12	0.83	2.85	70.5	Full	2

Table 4. Details of test specimen for transverse load test

Specimen number	Reinforcing bars for 1 grouted cell	Reinforcement ratio, ρ (%)	Span length, L (m)	Grouting pattern	No. of specimen
F1-237-P	2-DB12	0.27	2.37	Partial	2
F1-275-P	2-DB12	0.27	2.75	Partial	2
F2-237-P	2-RB9	0.23	2.37	Full	2
F2-275-P	2-RB9	0.23	2.75	Full	2
F3-237-P	2-DB16	0.48	2.37	Partial	2
F3-275-P	2-DB16	0.48	2.75	Partial	2
F4-237-P	2-DB12	0.41	2.37	Full	2
F4-275-P	2-DB12	0.41	2.75	Full	2

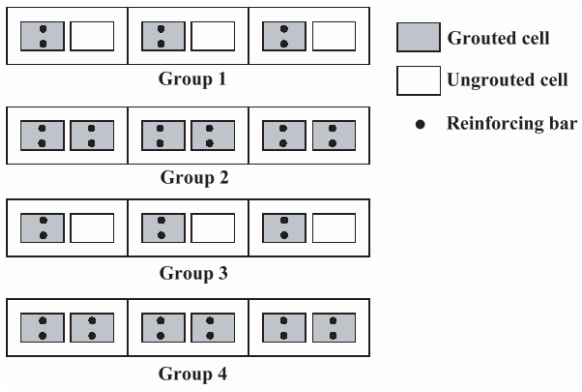

Figure 3. Cross-sections of the wall specimens

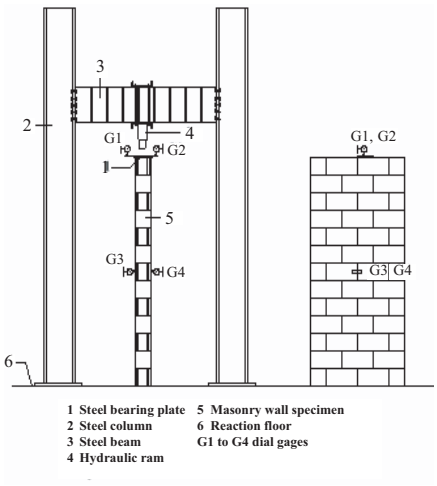

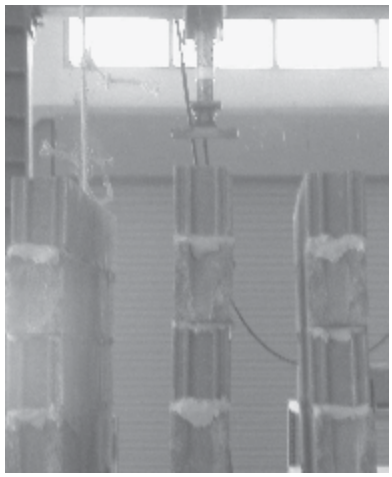

a) Schematic diagram b) Steel load-bearing plate and hinged support

Figure 4. Test set-up for concentrated axial load test

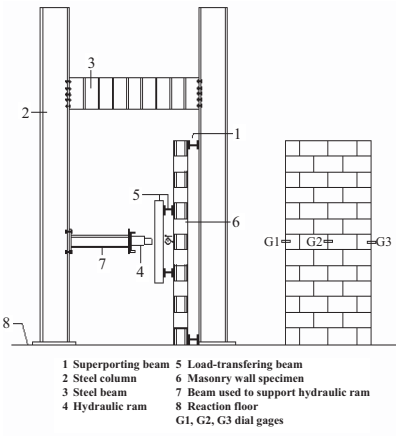

a) Schematic diagram b) Load-transferring system

Figure 5. Test set-up for transverse load test

measured by three dial gages; one at the center and one at each of the two edges. According to the test results obtained in the prism test, a preload of 30% of the estimated ultimate loads was applied before the beginning of the test to settle down the uneven bed surfaces of the masonry units and then unloaded to about 2 kN to seat the specimen into the testing position. All specimens were tested to failure.

Results and Discussions

Behavior and Mode of Failure of the Specimens under Concentrated Axial Load

During the preloading, it was observed that cracks developed randomly in the test specimens due to the uneven surfaces of the masonry units, similar to that observed in the prism tests. These cracks can be classified into two types. The first type is due to load transfer caused by unequal friction that obstructs lateral deformation of the masonry units. These cracks developed along the edges of the head joints and extended through the masonry units above and below as shown in Figure 6(a). The second type is due to flexural movements caused by height tolerances of the masonry units in a course. These cracks developed along the edges of the head joints and extended through the masonry units below as shown in Figure 6(b). These flexural cracks were usually accelerated when a higher load was applied until a full contact between the masonry units was achieved.

Figure 7 shows a typical plot of the axial load-axial deformation for the concentrated axial load test. The specimens showed a linear response up to 65 - 80% of the ultimate axial load. When

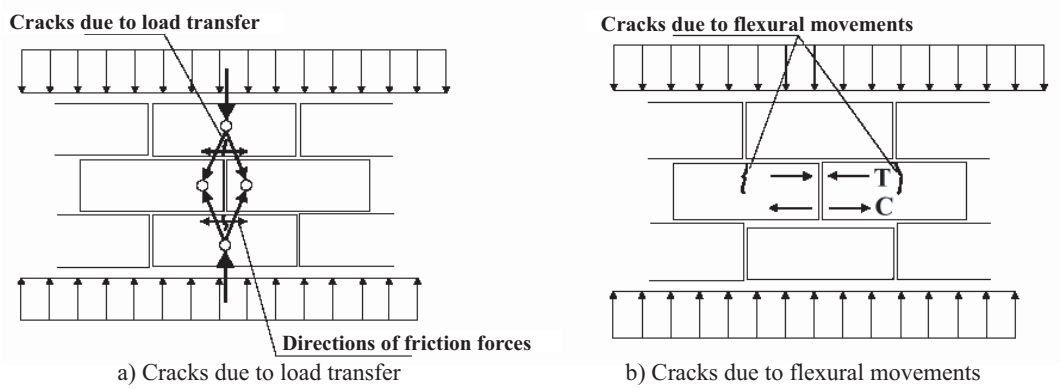

a) Cracks due to load transfer b) Cracks due to flexural movements

Figure 6. Cracks due to the uneven bed surfaces of the units

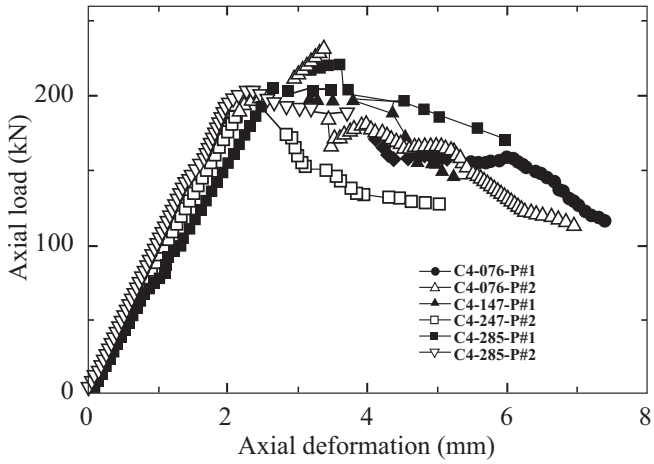

Figure 7. Typical axial load-axial deformation curves for concentrated axial load test

the applied load within this linear range was increased, the cracks observed during preloading continued to increase in size but did not influence the response of the specimens. As the load approached the linear limit, vertical cracks occurred on the face shell directly in line with the edges of the bearing plate. These cracks were formed by the bearing plate tearing against the masonry. On a further increase of the applied load beyond the linear limit, the slope of the curve decreased until the applied load reached the ultimate load. Finally, the applied load dropped with a significant increase in the axial deformation. Generally, specimens failed by a tearing and crushing of the masonry in the region beneath the bearing plate with a shear line in the diagonal direction. The shear line extended from the bearing plate along the specimen height at an angle of 20 to 30 degrees to the vertical for fully grouted specimens and at an angle of 25 to 35 degrees for partially grouted specimens as shown in Figure 8. Differences in the shear line angles indicate that the grout and reinforcing bars can reduce the magnitude of the load dispersion angle under the bearing plate. It should be noted that these angles are more severe than the frequently assumed value of 45 degrees typically used in design, since the masonry area supporting the

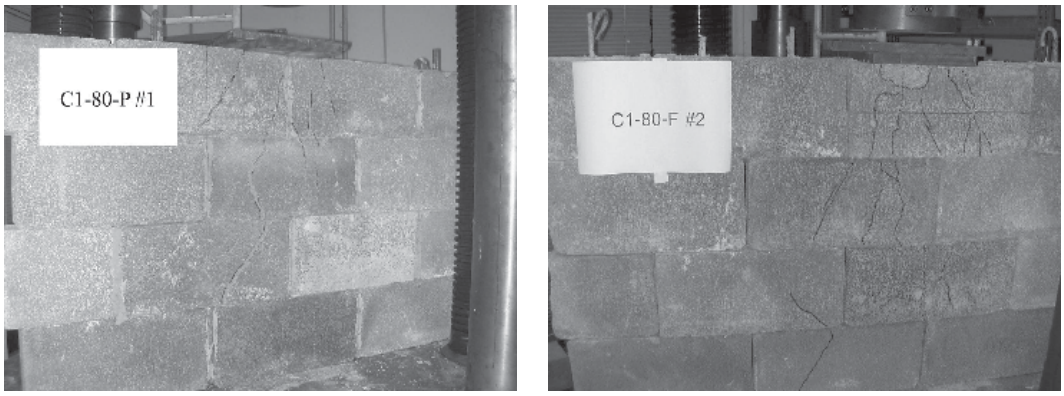

a) Partially grouted specimen b) Fully grouted specimen

Figure 8. Cracks in the test specimens due to concentrated axial loads

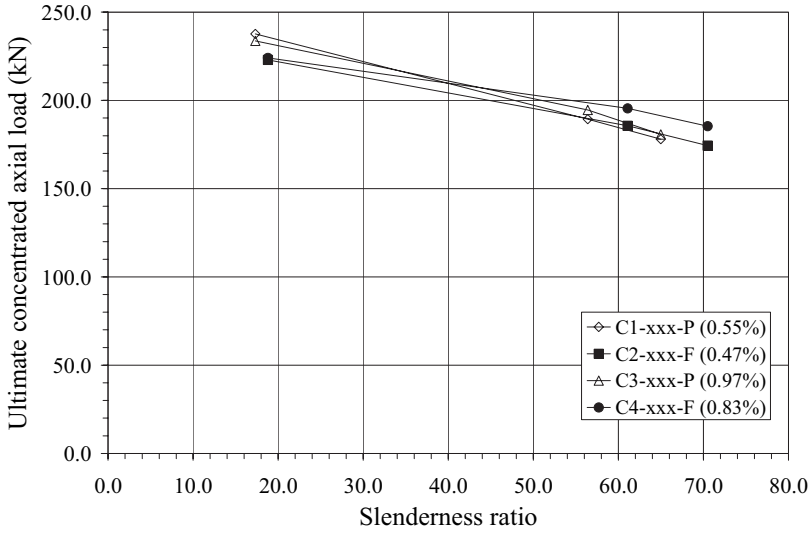

Figure 9. Ultimate concentrated axial load versus slenderness ratio

applied load was reduced by nearly 50% (Page and Shrive, 1990).

Figure 9 shows a typical plot of the ultimate concentrated axial load versus slenderness ratio. Increasing the slenderness ratio decreased the ultimate axial loads slightly. Since all specimens failed in the same mode as described in the previous paragraph, the decrease in the ultimate axial load must have been due to unavoidable factors such as misalignment of the specimen, the specimen's out-of-straightness, and eccentricity of the applied load. It was also found that increasing the reinforcement ratio and grouting area did not increase the ultimate loads. This insensitivity of the ultimate loads is due to the fact that all specimens have an equal load-bearing area and the reinforcing bars yielded at a strain well below the ultimate strain of the masonry. In addition, by examining the cracks in the region under the bearing plate, it was found that no crack extended passing the head joint to the adjacent masonry units in the same course. This indicates that there was no stress transfer through the head joint. Therefore, the plate bearing area should be used to calculate the ultimate stress of the wall specimens.

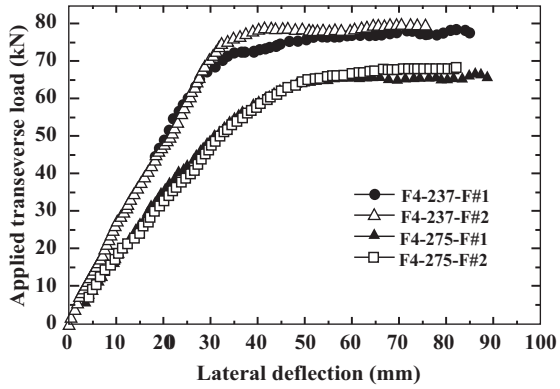

Figure 10. Typical applied transverse load versus lateral deflection

a) Crushing lines on the compression surface

b) Deflected shape at failure

Figure 11. Typical mode of failure of the specimens due to transverse loads.

Behavior and Mode of Failure of the Specimens under Transverse load

During the preloading, it was observed that the specimens had an initial deflection in the first load level up to 5 - 10% of the maximum transverse load. Figure 10 shows the typical curves of the applied transverse load versus lateral deflection at mid-span. Generally, the curves consist of two linear segments, indicating that the specimens had a bilinear behavior with a larger stiffness in the first linear segment. Following the flexural analysis for the reinforced masonry wall presented in Matthys (1993), it was found that the tensile steel reinforcing bars yielded near the end of the first linear segment, thus reducing the stiffness of the second linear segment. In addition, large tensile cracks along the bed surfaces between the masonry units and large deflection at the mid-span were observed. Therefore, in this study, the bending moment due to the transverse load that causes the yielding of the tensile steel reinforcing bars was taken as the flexural strength of the masonry specimen. At the end of the tests, the maximum transverse loads were in the range of 10% to 25% greater than that

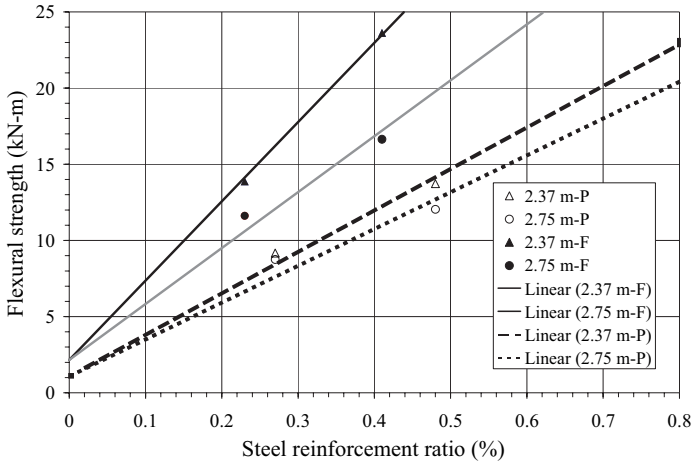

Figure 12. Flexural strength versus steel reinforcement ratio

Table 5. Observed ultimate load, ACI and proposed allowable axial loads, and their ratios

Specimen number	P_{ult} (kN)	P_a (kN)	P'_a (kN)	P_{ult}/P_a	P_{ult}/P'_a
C1-076-P	237.7	65	56.1	3.66	5.95
C1-247-P	189.3	55.3	47.8	3.42	5.57
C1-285-P	178	51.8	44.7	3.44	5.6
C2-076-F	222.9	88.2	74.9	2.53	3.7
C2-247-F	185.6	72.7	61.7	2.55	3.74
C2-285-F	174.4	67.1	56.9	2.6	3.81
C3-076-P	233.7	86.8	78	2.69	5.85
C3-247-P	194.6	73.9	66.3	2.63	5.73
C3-285-P	180.7	69.2	62.1	2.61	5.68
C4-076-F	224.1	108.1	94.7	2.07	3.72
C4-247-F	195.4	89.1	78.1	2.19	3.94
C4-285-F	185.4	82.2	72	2.26	4.05

of the yielded transverse load. All specimens failed with large tensile cracks along the bed surfaces of the masonry units on the tension zone of the specimens and crushing of the masonry units on the compression surface as shown in Figure 11.

Figure 12 shows the plot of the flexural strength versus steel reinforcement ratio for different span lengths and grouting patterns. The flexural strength at zero reinforcement ratio was calculated using the modulus of rupture of the grout and the classical flexural formula. The modulus of rupture was determined by using 9 grout specimens according to ASTM C78 and was found to be 2.024 MPa. Using linear regression analysis, it can be seen that the relationship between the flexural strength and the steel reinforcement ratio is linear, which is in good agreement with the flexural theory in Matthys (1993). As expected, increasing the steel reinforcement ratio and the grouting area increase the flexural strength, but increasing the span length decreases the flexural strength.

Comparisons of the Concentrated Axial Load Test Results with the Design Equations.

Table 5 shows the observed ultimate axial load, P_{ult}, along with the allowable axial load, P_a, the proposed allowable axial load, P'_a, and the ratios of the ultimate axial load to the allowable

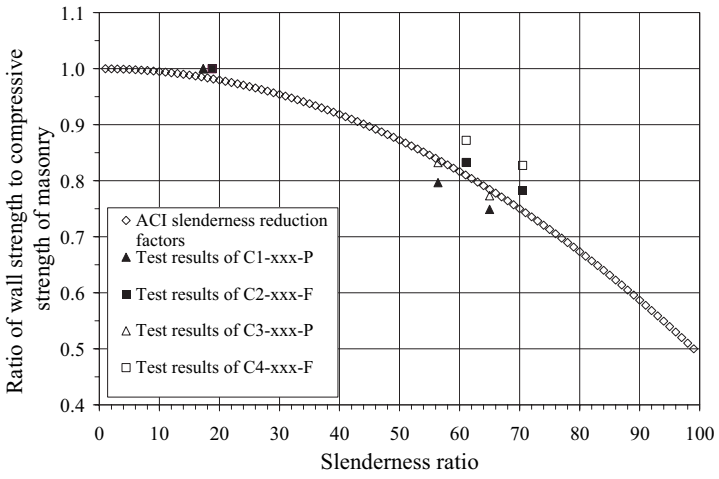

Figure 13. Ratio of wall strength to compressive strength of masonry versus slen dernessratio

Table 6. Experimental flexural strength, ACI and proposed allowable moments, and their ratios

Specimen number	M_{exp} (kN-m)	M_a (kN-m)	M'_a (kN-m)	M_{exp}/M_a	M_{exp}/M'_a
F1-237-P	9.17	4.16	3.71	2.21	2.47
F1-275-P	8.75	4.16	3.71	2.1	2.36
F2-237-F	13.88	4.74	4.74	2.93	2.93
F2-275-F	11.62	4.74	4.74	2.45	2.45
F3-237-P	13.73	6.54	4.43	2.1	3.1
F3-275-P	12.04	6.54	4.43	1.84	2.72
F4-237-F	23.63	8.17	6.19	2.89	3.82
F4-275-F	16.64	8.17	6.19	2.04	2.69

load. Since the slenderness ratios of the specimens used in this study were less than 99, the ACI allowable axial load was calculated by using the equation

$$P_a = (0.25 f'_m A_n + 0.65 A_{st} F_s)\left[1 - \left(\frac{h}{140r}\right)^2\right] \quad (1)$$

where f'_m is the compressive strength of the masonry prism, depending on the grouting pattern, A_n is the net cross-sectional area, A_{st} is the area of reinforcing bar, F_s is the allowable compressive stress of the reinforcing bar, and h/r is the slenderness ratio of the specimen. In this study, the value of f'_m was determined from the prism test without multiplying with the height-to-thickness correction factor and A_n was calculated from the load bearing area. The values of F_s were shown in Table 2. It should be noted, Eqn. (1) was developed by using the factor of safety of 4.0 and 3.85 against the failure of the masonry prism and the reinforcing bar, respectively.

From Table 5, the ratios of the observed ultimate load to the allowable load are in the range of 2.07 and 3.66 with an average of 2.72 and a coefficient of variation (COV) of 0.19. Performing the normality test, the distribution of the ratios had the correlation (R-value) of 0.9374, which can be assumed as normal distribution. In practice, the probability of failure of the masonry walls (the probability that the masonry walls have the ratios of the ultimate load to the allowable load less than 1.0) is usually set to be at least 1/10,000 (Harr, 1987). This probability value corresponds to a reliability of 99.99% and a reliability index of 3.72. By analyzing the data, the probability of failure of the wall specimens under concentrated axial load was found to be 1/2460, which is over 4 times greater than the recommended value. In addition, the mean value of the ratios is quite low compared to the factor of safety of 3.0 to 4.0 which is used in deriving the allowable stress design equation for the masonry wall under axial load. Therefore, the ACI equation should be modified for the mortarless reinforced concrete masonry wall.

Apart from the lack of mortar, there are a number of unavoidable factors that reduce the axial ultimate load of the masonry walls such as load eccentricity, member misalignment, and the memberís out-of-straightness. These factors are associated with the slenderness ratios of the walls, and their ultimate load reduction effects were included in the slenderness-reduction factor. To examine this effect, the dimensionless ratio of the wall strength to the compressive strength of the masonry was plotted against the slenderness ratio as shown in Figure 13. The compressive strength of the masonry was taken as the averaged nominal bearing strength of the specimens 0.76 m high. It was found that the calculated ratios compare well with the curve of the ACI strength-reduction factor. Therefore, it can be assumed that the slenderness-reduction factor of the mortarless masonry walls has the form of the ACI slenderness-reduction factor.

From Table 5, it can be seen that increasing the reinforcement ratio and grouting area decreased the ratios of the ultimate axial load to the allowable axial load considerably. This is due to the fact that Eqn. (1) includes both factors in the prediction of the allowable axial load. From the test results, however, neither factor influenced the bearing load capacity of the wall specimens. This may be due to the lack of enough lateral support from the stirrups, especially those directly under the bearing plate. Therefore, the steel reinforcements were buckled long before reaching the yielding point and they can only support a small portion of the applied load. The buckle of the steel reinforcements was clearly seen after the failure of the wall specimens. In addition, all specimens had the same load bearing area and failed in the same crushing and tearing mode. Therefore, it was concluded that the contribution of reinforcing bars to the bearing strength of the mortarless masonry wall is small and should be neglected. The bearing strengths were found to be 8.45 and 11.32 MPa for specimen groups 1 and 3 (partially grouted specimens) and 8.30 and 10.67 MPa for specimen groups 2 and 4 (fully grouted specimens). These values were typically lower than the compressive strength of the mortarless masonry prisms as shown in Table 1. This indicates that there is no confinement of the bearing area by surrounding grout and masonry and that there is stress concentration under the bearing area. Therefore, the design rules for the concentrated load distribution specified in ACI

530-99 should not be applied for the mortarless masonry in this case. However, as shown in Page and Shrive (1990), the bearing strength can be increased by using a bond beam and/or larger bearing plate. This problem requires further investigation.

There are a number of factors that contribute to the variations in the compressive strength of the masonry prisms such as the variation in the dimensions, in the material properties, and in the construction practices. In this study, the variation in the dimensions was considered to be the major factor that gives a higher variation of the compressive strength of the mortarless masonry prisms compared with the variation of the mortar jointed prism. Based on the statistical analysis of the data obtained in Seangatith and Chaijaruwanich, 2001, the COV of the mortar jointed prism was found to be 0.15 and since there is a limit number of test data in this study, the COV of the compressive strength of the mortarless prisms was assumed to be 0.20, which is 33% larger than that of the mortar jointed prism. Therefore, the factor of safety associated with the compressive strength of the masonry prism should be increased from 4.0 to 4.44, which is similar to that used in the EIT 1005-75. Therefore, the proposed design equation should be in the form of(2) From Table 5, Eqn. (2) gives the ratio of the ultimate load to the allowable load between 3.70 and 5.95 with an average of 4.78 and a COV of 0.21, which is larger than the recommended factor of safety of 3.0 to 4.0. Performing the normality test, it was found that the distribution of the ratios can be assumed as a normal distribution with an R-value of 0.8891. Thus, the probability that the ratio is less than 1.0 is about 1/12,000 with the reliability index of 3.77.

Comparisons of the Transverse Load Test Results with the Design Equations

Table 6 shows the experimental flexural strength, M_{exp}, the allowable moment, M_a, the proposed allowable moment, M'_a, and the ratios of the tested flexural strength to the allowable moment. The allowable moment was calculated from the flexural equations in Matthys (1993). It was taken from the smaller of the moment controlled by the allowable flexural compressive strength of the masonry, M_m, and the moment controlled by the allowable tensile strength of the steel reinforcing bar, M_t, where

$$M_m = \frac{b_e d^2 k j F_b}{2} \qquad (3)$$

$$M_t = A_s j d F_s \qquad (4)$$

where b_e is the effective width for a reinforcing bar and is taken as the center-to-center distance of the reinforcing bars, d is the distance from the compressive surface of the masonry wall to the reinforcing bar, k can be calculated from $k = \sqrt{(n\rho)^2 + 2n\rho} - n\rho$, where n is the modular ratio which is the ratio of the modulus of elasticity of the steel and masonry and ρ is the steel reinforcement ratio, j can be calculated from , $j = 1-(k/3)$, F_b is the allowable flexural compressive strength of the masonry, equal to $(1/3)f'_m$, and F_s is the allowable tensile stress of the reinforcing bar. It should be noted that the factor of safety of 3.33 of F_b in Eqn. (3) is determined from the test data in which the compressive stress at failure for hollow masonry subjected to flexure is larger than that for the masonry under axial load by 33% (Commentary on Building Code Requirements for Masonry Structure, 1999). The factors of safety of F_s are 2.0 for steel grade 40 and 50 and 2.5 for steel grade 60.

Table 6 shows that the ratio of the tested flexural strength to the allowable moment ranges between 1.84 and 2.93 with an average of 2.32 and a COV of 0.17. Performing the normality test, the distribution of the ratios can be assumed to be a normal distribution with an R-value of 0.9468. The probability of failure of the ratios is 1/1,950, which is more than 5 times larger than the recommended value. In addition, the mean value of the ratio is quite low compared with the factor of safety of 2.5 to 3.0 generally used in the development of the allowable stress design equation for masonry wall under flexure (Matthys, 1993). Therefore, the equations for a mortarless reinforced concrete masonry wall should be modified.

Due to the lack of test data to confirm the increase in the flexural compressive strength of

the mortarless masonry compared with the axial compressive strength and to account for the quality of the masonry units, the factor of safety for F_b in Eqn. (3) should be the same as that for f'_m for axial compression. Using this allowable flexural compressive strength, it can be seen that the ratio of the flexural strength to the allowable moment is in the range of 2.36 and 3.82 with an average of 2.82 and a COV of 0.17. This is in good agreement with the recommended factor of safety. Performing the normality test, it was found that the distribution of the ratios fits normal distribution with an R-value of 0.9252. The probability that the ratio is less than 1.0 is 1/14,700 with the reliability index of 3.82.

Conclusion

From the study, the following conclusions can be drawn.

1. The mortarless masonry wall specimens under concentric axial load showed large initial deformation soon after loading to about 35% of the compressive strength due to the uneven surfaces of the units. Two types of cracks were also observed during this initial loading: cracks due to load transfer caused by unequal friction that obstructs lateral deformation of the masonry units and cracks due to flexural movements caused by height tolerances of the masonry units in a course. They occurred until full contact between the masonry units was reached. However, this initial deformation is quite small for the specimens under transverse loads.

2. The relationship of concentric axial load and axial deformation was linear up to 65 - 80% of the ultimate axial load. Failure was due to tearing and crushing of the masonry in the region beneath the bearing plate with a shear line in a diagonal direction extending from that region along the specimen height. The shear line angle was 20 to 30 degrees to the vertical for fully grouted walls and 25 to 35 degrees to the vertical for partially grouted walls. Therefore, the design rules for concentrated load dispersion specified in ACI 530-99 should not be applied for the mortarless masonry in this case. Due to this failure mode, increasing the steel reinforcing area and grouting area do not increase the ultimate bearing strength of the walls.

3. The relationship of transverse load to mid-span deflection is bilinear with a larger stiffness in the first linear segment. At the end of the first linear segment, large deflection at the mid-span of the wall with a yielding of steel reinforcement was observed. Failure was due to crushing of the masonry units on the compression surface with large tensile cracks on the tension zone. Increasing the steel reinforcing area and grouting area increase the flexural strength, which is in accordance with the results from the design equations.

4. For concentrated axial load, the design equation should be in the form of Eqn. (2). This equation gives a ratio of the ultimate load to the allowable load in the range of 3.70 and 5.95 with an average of 4.78 and a COV of 0.21. For transverse load, Eqn. (3) with the flexural allowable compressive strength of $F_b = 0.225f'_m$ and Eqn. (4) should be used. These equations give the ratio of the flexural strength to the allowable moment in the range of 2.36 and 3.82 with an average of 2.82 and a COV of 0.17.

Acknowledgement

The research work presented in this paper has been sponsored by Suranaree University of Technology under the project number SUT7-712-47-12-05; this support is gratefully acknowledged. The author also would like to thank Assoc. Prof. Dr. Amnat Apichatvullop for his suggestions. The results presented herein represent the views and opinions of the writer only.

References

Building Code Requirements for Masonry Structures (ACI 530-99/ASCE 5-99/TMS 402-99). (1999). Masonry Jointed Committee. American Concrete Institute/American Society of Civil Engineers/The Masonry Society, CO., p. 104.

Commentary on Building Code Requirements for Masonry Structure (ACI 530-99/ASCE 5-99/TMS 402-99). (1999). Masonry

Jointed Committee. American Concrete Institute/American Society of Civil Engineers/The Masonry Society, CO., total number of pages.

Harr, M.E. (1987). Reliability-Based Design in Civil Engineering. 1st Ed. McGraw-Hill. NY, USA, total number of pages.

Marzahn, G. (1997). Dry-Stacked Masonry in Comparison with Mortar Jointed Masonry. LACER, 2:353-365.

Marzahn, G. (1999). Investigation on the Initial Settlement of Dry-Stacked Masonry under Compression. LACER, 4:253-270

Marzahn, G. (2000). A Study on the Creep Behavior of Dry-Stacked Masonry Walls and Individual Masonry Units. LACER, 5:261-278.

Matthys, J.H. (1993). Masonry Designer,s Guide. The Masonry Society, CO., USA, total number of pages.

Page, A.W., and Shrive, N.G. (1990). Concentrated loads on hollow concrete masonry. ACI Structural Journal, 87(4):436-444.

Standard Specification for Loadbearing Concrete Masonry Units. (2000). C90-00. ASTM. West Conshohoken, PA, total number of pages.

Standard Specification for Grout for Masonry. (1999). C476-99. ASTM. West Conshohoken, PA, total number of pages.

Standard Specification for Deformed and Plain Billet-Steel Bars for Concrete Reinforcement. (2004). A615-99. ASTM. West Conshohoken, PA, total number of pages.

Standard Test Methods for Sampling and Testing Concrete Masonry Units and Related Units. (1999). C140-99b. ASTM. West Conshohoken, PA, total number of pages.

Standard Test Method for Sampling and Testing Grout. (2000). C1019-00b. ASTM. West Conshohoken, PA, total number of pages.

Test Methods for Compressive Strength of Labo ratory Constructed Masonry Prisms. (1997). E447-97. ASTM. West Conshohoken, PA, total number of pages.

Standard Test Methods for Tension Testing of Metallic Materials. (2000). E8-00b. ASTM. West Conshohoken, PA, total number of pages.

Standard Specification for Mortar for Unit Masonry. (2000). C270-00. ASTM. West Conshohoken, PA, total number of pages.

Standard Test Method for Flexural Strength of Concrete (Using Simple Beam with Third-Point Loading). (2000). C78-00. ASTM. West Conshohoken, PA, total number of pages.

Seangatith, S., and Chaijaruwanich, J. (2001). Compressive Strength of Concrete Masonry Units and Prisms. Suranaree J. Sci. Technol., 8(3):131-137.

Standard for Masonry Structures (EIT 1005-75). (1975). Engineering Institute of Thailand, Bangkok, total number of pages.